



PAPER

OPEN ACCESS

RECEIVED

16 February 2018

REVISED

3 April 2018

ACCEPTED FOR PUBLICATION

27 April 2018

PUBLISHED

9 May 2018

Original content from this work may be used under the terms of the [Creative Commons Attribution 3.0 licence](https://creativecommons.org/licenses/by/3.0/).

Any further distribution of this work must maintain attribution to the author(s) and the title of the work, journal citation and DOI.



Microstructure and magneto-optical surface plasmon resonance of Co/Au multilayers

Conrad Rizal¹ , Simone Pisana^{1,4} , Ivan Hrvoic² and Eric E Fullerton³¹ Department of Electrical Engineering and Computer Science, York University, 4700 Keele Street, Toronto, ON, M3J 1P3, Canada² GEM Systems Inc, 135 Spy Court, Toronto, ON, L3R 5H6, Canada³ Center for Memory and Recording Research, University of California, San Diego, 9500 Gilman Dr, La Jolla, CA, 92093, United States of America⁴ Author to whom any correspondence should be addressed.E-mail: crizal@yorku.ca, simone.pisana@lassonde.yorku.ca, ivan@gemsys.ca and efullerton@ucsd.edu**Keywords:** surface plasmon resonance, Co/Au, magneto-optics surface plasmon resonance, biosensor, microstructure

Abstract

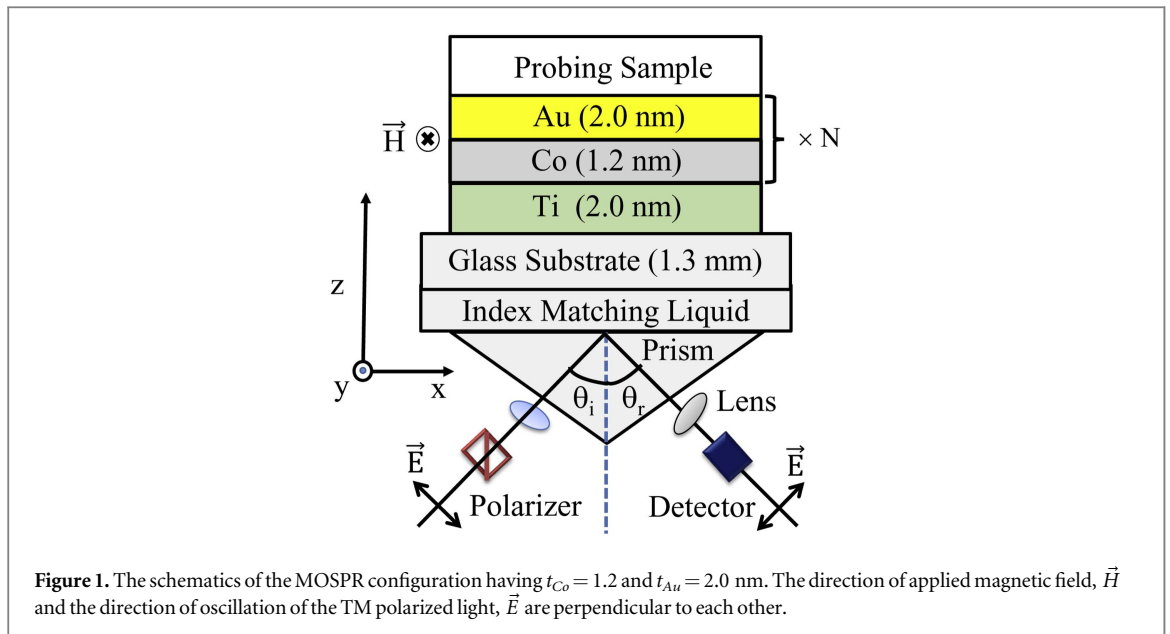
Magneto-optical surface plasmon resonance (MOSPR) sensors benefit from a magneto-optic enhancement with respect to surface plasmon resonance (SPR) sensors, making these devices attractive for biosensing applications. Typical design compromises seek to balance magneto-optic effects and optical losses associated with surface plasmon waves extending to the ferromagnetic layer. Here, we demonstrate that Co/Au multilayers can yield sizeable MOSPR improvements in spite of the relative high total Co layer thickness. Co (t_{Co})/Au (2 nm) multilayers, with $1.2 \leq t_{Co} \leq 1.8$ nm are prepared and characterized. X-ray analysis shows that the microstructure maintains high layer periodicity and improves upon annealing. The multilayer structures were then modeled to study their SPR/MOSPR sensitivities, suggesting that the MOSPR sensitivity is enhanced by a factor of up to 3 and 4 with respect to the SPR sensitivity when the devices are operated in Air and Water media, respectively. We find that multilayers provide a particular advantage when operating the sensors in Water-based media.

1. Introduction

Co/Au multilayers (MLs) are of great interest not only due to their magnetic and magneto-optic properties, but also due to the plasmonic enhancement that is associated with Au, making them attractive for application in magnetic-recording and ultra-sensitive biosensors. If deposited and annealed under controlled conditions their microstructural, optical, and magneto-optical (MO) properties can be changed and tuned substantially [1–5]. From the prospective of designing more efficient MO devices, these MLs offer the possibility of carefully tuning the plasmonic properties of the diamagnetic layer, in this case Au, with the MO effect of the ferromagnetic layer, in this case Co. This increased degree of freedom opens new avenues for improving state of the art surface plasmon resonance (SPR) biosensors, by balancing optical losses detrimental to plasmon resonance against the MO enhancement associated with the resistive Co layer. We recently reviewed *biomagnetoplasmonics* (see, [6]), using the SPR phenomena and discussed their potential to use as sensor in wide range of applications. We focused on Ti (2 nm)/Co (10 nm)/Au (35 nm) structures, and highlighted that by using thin Co layers small saturating fields $H_s \approx 50$ Oe can be used to modulate the MO effect and enhance SPR signals. On the other hand, the flexibility afforded by magnetic MLs allows to tune the magnetic anisotropy and other magnetic properties of the sensor [7].

Ignatyeva *et al* have shown a marked enhancement in magneto-optic SPR (MOSPR) effects via a photonic crystal structure [2]. In their work, Co/Au bilayers of the kind typically employed in SPR sensors are coupled to a photonic crystal, effectively trapping the surface plasmon wave and increasing its propagation distance, thereby narrowing the resonance condition, with an associated increase in sensitivity by a factor of 7.

Armelles *et al* have reported a series of studies on MO enhancements in a variety of magnetoplasmonic structures [8]. Layer thickness optimization in Au/Co/Au trilayers leads to a compromise between MO



enhancements and optical losses. However, periodic MLs have not been studied for MOSPR applications, and may provide a better compromise.

In the past we reported on giant magnetoresistance, magnetic anisotropy, and micro-structure properties of a series of Co-based multilayers and alloys, using a variety of deposition techniques [7, 9–12]. These structures exhibited strong microstructure-dependent magnetic anisotropy, which was found to be controllable and tunable by tuning the surface structure, layer thickness, and annealing/magnetic annealing conditions.

In the present work, we employ MLs composed of repeats of Co (t_{Co})/Au (2 nm), where $1.2 \leq t_{Co} \leq 1.8$ nm, in a SPR transducer configuration. We first focus on structural morphology of the MLs, demonstrating their high periodicity. Then we model these structures and the influence of layer thickness and periodicity on the SPR and MOSPR responses, comparing the performance in terms of sensitivity in air or water media.

2. Material and methods

Co/Au MLs with constant Au layer thickness ($t_{Au} = 2$ nm) and varying Co layer thickness ($1.2 \leq t_{Co} \leq 1.8$ nm) were deposited onto a 2-nm Ti buffer layer on glass substrates by dc-magnetron sputtering at ambient temperature and at a pressure of 6×10^{-8} Torr. The MLs consisted of 20 Co/Au repeats and were subsequently annealed at 400 °C for 30 minutes. A Rigaku Smart Lab diffractometer, with Cu-K α radiation of $\lambda = 0.154$ nm and with three resolution-defining slits, was employed for x-ray diffraction (XRD) and x-ray reflection (XRR) analysis.

The simplest way to describe surface plasmons is to treat each material as a homogeneous continuum, in which the material's dielectric constant has a complex-valued permittivity. For surface plasmons to exist, the real part of the dielectric constant of the metal must be negative and its magnitude must be greater than that of the dielectric. This condition is met in the IR-visible wavelength region for noble metal/dielectric interfaces.

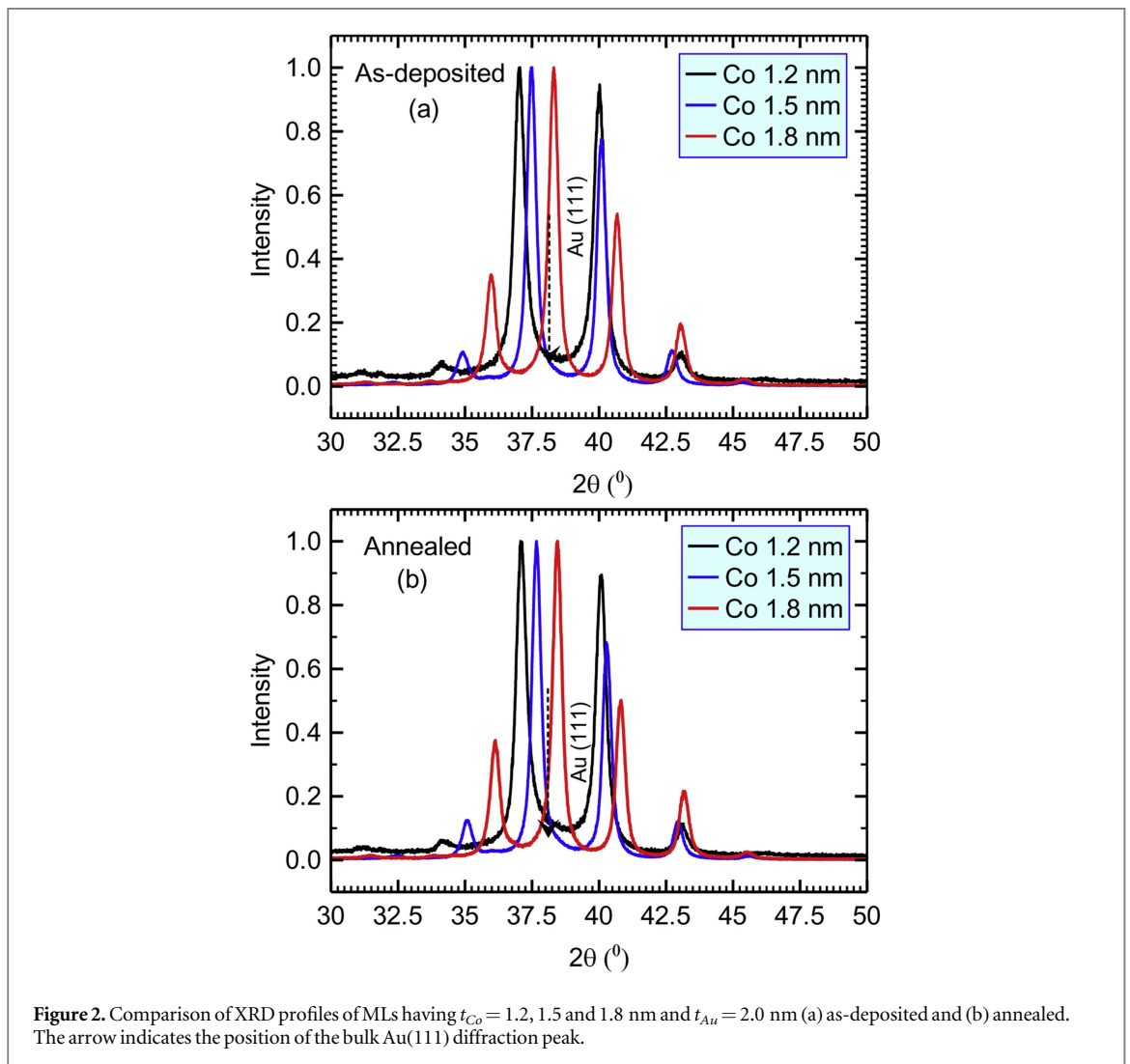
The prism-coupled *Kretschmann configuration* was employed to excite surface plasmons similarly to [13]), see figure 1. A transfer-matrix formalism was used in Lumerical FDTD to model the excitation of surface plasmons leading to resonance. As shown in figure 1, the direction of applied magnetic field, H ($0.5 \text{ kOe} \leq H \leq 1.0 \text{ kOe}$) is kept parallel to the Co/Au interface and perpendicular to the plane of incidence of the optical radiation, which is TM or p -polarized. The parameters used for the calculations are given in table 1.

3. Results and discussions

Nanoscale MLs show layer periodicity at length scales that are comparable to or larger than the atomic spacing of bulk materials, so naturally x-ray diffraction (XRD) and x-ray reflection (XRR) techniques are extensively employed to investigate the structural properties of these kinds of MLs. XRD offers structural information such as crystallite size, lattice orientation and strain, deformation energy density, etc., whereas XRR offers information on individual layer thickness, ML periodicity and surface/inter-layer roughness [15]. Here we

Table 1. Optical properties of metals and dielectrics at $\lambda = 785$ nm. $\epsilon_{mo(\text{Co})}$ is the magneto-optic constant of Co, and was obtained from [14].

Material	t (nm)	ϵ_{xx}	ϵ_{mo}
Au	2	$-22.85 + j01.44$	—
Co	1.2	$-16.49 + j23.38$	$-0.85 + j0.0006$
Ti	2	$-6.51 + j24.81$	—
Air	—	1.00055	—
He	—	1.00007	—
Water	—	1.76780	—
Methanol	—	1.72960	—
Glass	1300	2.28130	—



summarize the results, but for further detail on the microstructure of these continuous MLs and their magnetic characteristics, we refer the reader to our prior work [7].

3.1. X-ray diffraction analysis

The x-ray diffraction (XRD) spectra of the Co/Au MLs is given in figure 2: (a) as-deposited and (b) annealed. As shown for the as-deposited samples, a variation in both the peak position as well as intensity and full-width at half-maximum (FWHM) is observed with varying Co layer thickness (t_{Co}). The peak position shifted significantly towards higher angles with t_{Co} , which is associated with a decrease in average crystal grain size (D), as grain size varies inversely with $\cos \theta$. The decrease in D with t_{Co} in turn is attributed to an increase in tensile strain in the lateral direction, as lateral strain varies proportionally to $\tan \theta$ [7, 16].

As shown for the annealed samples, changes were observed in both peak position, intensity, and FWHM, suggesting changes in grain size as well as the state of strain. The broadening of peak width, β , at FWHM indicates that the lattice constant or unit cell size decreased, as D and β are inversely related through Scherrer's formula as $D = \lambda K / \beta \cos \theta$, where K is a constant (≈ 0.97) [17]. The out-of-plane lattice spacing on the other hand is inversely related to $\sin \theta$, which means it increases as the peak position shifts to the right. The result suggests that the compressive strain along the vertical direction decreased due to annealing [7].

All the measured XRD profiles in (a) and (b) showed two dominant peaks and two satellite peaks. As shown, the dominant peaks appeared around 37° and 40° , whereas the satellite peaks appeared around 35° and 43° (for $t_{Co} = 1.2$ nm). For higher t_{Co} these peak positions are shifted to higher angles. We attribute the intense peak at 37° to the Au (111) fcc-phase. This shift of diffraction peak towards lower angle from the bulk diffraction peak for Au (111), which is 38.2° , implies that the crystallite thickness decreased in MLs as opposed to bulk [15].

Another interesting aspect of these Bragg peaks is that they show a repeating pattern. The fact that these 4 peaks appear at the same interval of $\approx 3^\circ$ signifies the presence of a periodicity that dominates the diffraction of these MLs (as opposed to layer composition dominating the pattern). This pattern is attributed to the high bilayer periodicity in our MLs, which gives rise to the periodic refractive index difference between each Co/Au repeat. The angular separation of the satellite peaks is commensurate with the ML periodicity, and increases as t_{Co} is decreased, as $\sin(\theta_S) = \sin(\theta_B) \pm m \times \lambda / (2 \times P)$, where θ_S and θ_B are the positions of the satellite and Bragg peaks, respectively, m is the reflection order (1, 2, 3, ...), λ is the x-ray wavelength, and P , which is given by $t_{Co} + t_{Au}$, is the bilayer/period thickness. The reflection peaks due to Co are not observed here as the density of electrons contributing to Bragg reflections are much higher in Au compared to Co, and the intensity of reflections is proportional to electron density. The observation of the strong satellite peaks in both the as-deposited and annealed MLs suggests that they have strong structural coherence.

3.2. X-ray reflection analysis

Co layer thickness-dependent x-ray reflection (XRR) profiles of the Co/Au MLs are shown in figure 3: (a) as-deposited and (b) annealed samples. Both curves show distinct reflectivity profiles corresponding to the average inter-planar distance of Co and Au due to the constructive interference of the reflected beams from adjacent layers in the multilayer stack.

The peak positions for the annealed samples in (b) shifted slightly towards higher angles, as indicated by the right arrow, meaning that these MLs shrink slightly. The peak intensity on the other hand, increased with annealing, signifying improved interface quality (this is not explicitly visible in the normalized curves shown here).

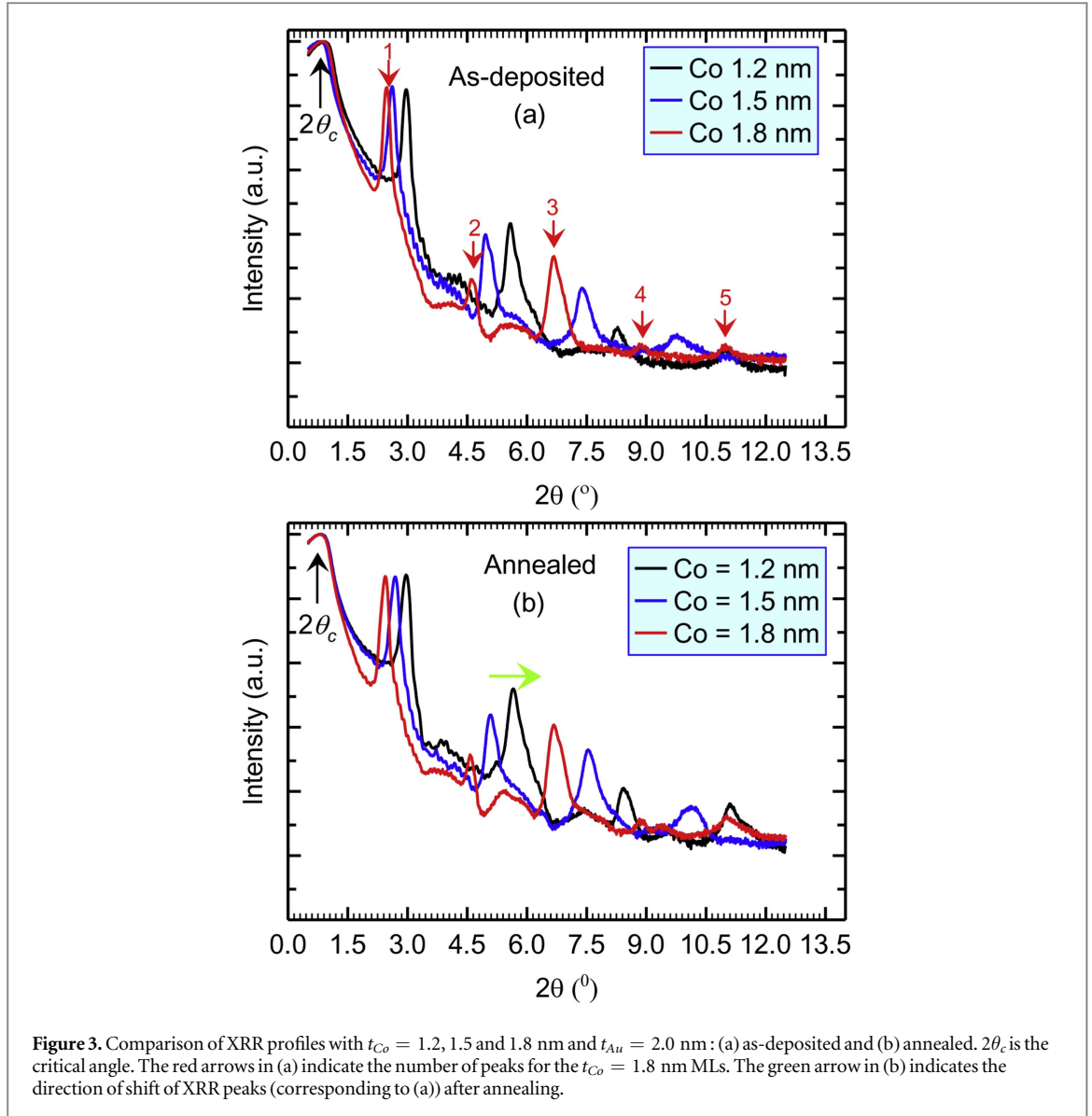
As shown, the presence of higher order Bragg peaks in XRR mode suggest that the MLs maintain good bilayer periodicity. The bilayer periodicity at low angle can be estimated using Bragg's law as $n\lambda = 2d \sin \theta$. The presence of the higher order Bragg peaks in XRR spectra further indicate that, despite the small layer thickness, all the samples studied here maintain good periodicity. The sharpening of the peaks upon annealing is an indication of improved periodicity due to the heat treatment.

From the comparison of XRR profiles of samples with different t_{Co} , as the t_{Co} increased, the roughness decreased for all samples, whereas the layer density increased, and with increasing density the inter-diffusion of atoms between adjacent layers markedly decreased [18].

A similar type of observation was reported by Dekadjevi *et al* [19] in the case of their Fe/Au ML system with a discontinuous low-density Fe layer deposited on a high-density Au layer. They reported a decrease in both the in-plane (also known as lateral) correlation length of both the interfaces and the perpendicular correlation length of the ML structure as the thickness of the Fe layer decreased. Comparison of the coherence length of our as-deposited and annealed samples suggested that, the in-plane correlation length increased by a factor of 1.3 at the interface after annealing.

The characteristic signature of bilayer periodicity is mainly defined and controlled by the relative difference in refractive index of the two materials, Au and Co. This is in turn determined by the atomic density and number of electrons per atom contributing to the scattering of the x-rays, also referred to as the scattering power of the material. Au, with more electrons, obviously possesses a stronger scattering power, so the property of the bilayer in this case is dominated by the reflections from Au layers. The reflections from bilayers is also influenced by interface roughness, which can be of two types—continuous and discrete. However, contributions from these two components are difficult to distinguish, hence these are usually expressed as total and overall roughness, given by $\sigma = \sqrt{(\sigma_c^2 + \sigma_d^2)}$, where σ_c and σ_d are continuous and discrete roughness, respectively [15].

The surface roughness of the multilayers with similar layer structure we estimated earlier is found to be 1.7 \AA and 0.2 \AA for Au and Co layers, respectively, and these values reduced to 1.5 \AA and 0.1 \AA upon annealing, suggesting small σ and clearer periodicities of our annealed multilayers. For further detail on roughness characteristics, we refer the reader to our prior work [7].



3.3. SPR and MOSPR analysis

The sensitivity of SPR sensors has been defined in many different ways in the literature [20]. The challenge in comparing reported values is that no single sensitivity metric is used.

In this work, the SPR sensitivity is calculated as,

$$S_{SPR} = \frac{R_{p(A)} - R_{p(B)}}{\Delta R_{p(A)m}} \times 100 \quad [\% \text{ RIU}^{-1}] \quad (1)$$

where, $R_{p(A)m}$ is the magnitude of reflected intensity at an incident angle θ_m where the first derivative $dR_p(\theta)/d\theta$ is maximized (the experimental condition that gives the best performance). The notation A and B in (1) denote the reflected intensity at θ_m for two different media with different permittivities.

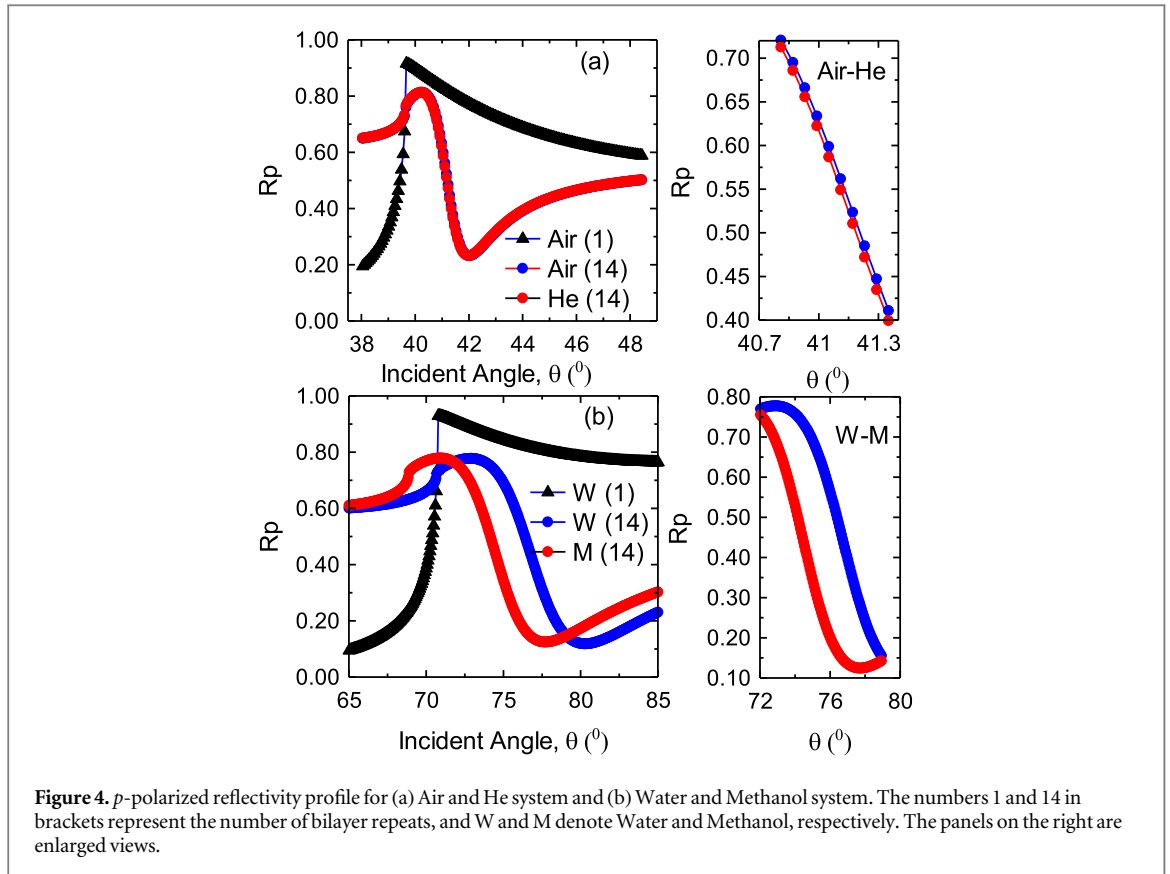
Similarly, the MOSPR sensitivity is calculated as:

$$S_{MOSPR} = \frac{\Delta R_{p(A)} - \Delta R_{p(B)}}{\Delta R_{p(A)m}} \times 100 \quad [\% \text{ RIU}^{-1}] \quad (2)$$

where the $\Delta R_{p(A)}$ and $\Delta R_{p(B)}$ are the changes in reflectivity due to modulating the H field for two different media A and B. $\Delta R_{p(A)m}$ is the maximum of the first derivative $d\Delta R_{p(A)}(\theta)/d\theta$.

These sensitivity metrics relate directly to the parameters measured and allow direct comparison of SPR vs MOSPR performance.

Figure 4 shows the SPR profiles for $[\text{Co } 1.2 \text{ nm}/\text{Au } 2 \text{ nm}] \times N = 1$ and 14 transducer configurations. The dielectric medium is varied from Air to He (a) and Water to Methanol (b). These variations in the sensed media are used to model variations in the refractive index associated with sensing. Both Air and Water media are shown



to highlight that a sensor optimized for a particular medium will not necessarily work equally well in a medium having a different average refractive index. Note that the change in refractive index for the Air to He variation is much smaller than that for Water to Methanol (see table 1), so the shift in the curves is smaller in the Air to He variation. However, the sensitivity metrics presented are normalized by the change in refractive index of the sensing medium, so the performance of the sensors can be directly compared between Air and Water media.

For the case of $[\text{Co } 1.2 \text{ nm}/\text{Au } 2 \text{ nm}] \times N = 1$ (a thin bilayer film), no sharp resonance is observed. Note however that the onset of total internal reflection (TIR, near 40° and 70° for Air and Water media, respectively) is very pronounced. We will return to this feature later, as the onset of TIR is also affected by the refractive index of the sensing medium, and can be used for sensing. For the case of $[\text{Co } 1.2 \text{ nm}/\text{Au } 2 \text{ nm}] \times N = 14$ (the ML structure fabricated), both the minimum reflectivity and peak positions are significantly different. We observe clear SPR characteristics for the $[\text{Co } 1.2 \text{ nm}/\text{Au } 2 \text{ nm}] \times N = 14$ ML with a minimum of around R_p of 0.22 in an Air medium and 0.12 for a Water medium. The SPR is also sharper for the Air medium compared to the Water. We also calculate the H field dependent reflectivity profiles. The excitation of surface plasmons in this case occurred at higher angles, and it is not shown here for clarity.

Figure 5 shows the SPR and MOSPR sensitivity profiles for $[\text{Co } 1.2 \text{ nm}/\text{Au } 2 \text{ nm}] \times N$ MLs in Air and Water media, calculated using equations (1) and (2) respectively. We also calculated the sensitivities of a thick $[\text{Co } 16.8 \text{ nm}/\text{Au } 28 \text{ nm}]$ reference bilayer, having total Co and Au layer thickness as that of the $N = 14$ ML, but the curves are not shown in figure 5 for simplicity. The sensitivity values obtained are summarized in table 2.

As shown, the $N = 10$ ML shows SPR sensitivity of $3.6 \times 10^4 \%$ /refractive index unit in Air, (RIU, a unit change in the refractive index of the medium of the sensor) and $1.8 \times 10^4 \%$ /RIU in Water. These sensitivities are lower than typical Au SPR sensors in Air ($5 \times 10^4 \%$ /RIU), and of optimized SPR sensors in Air ($10^5 \%$ /RIU) [2] consisting of a single thin Co/Au bilayer coupled to a photonic crystal structure. The relatively low sensitivity of the SPR ML sensors are a repercussion of the optical losses taking place when thick Co layers or many thin Co layers are present, which reduce the sensor performance, as expected. It's interesting to note that changes to the onset of TIR due to the variation in sensing medium refractive index leads to sensitivities comparable to the $N = 10$ ML. For the MOSPR configuration, the $N = 5$ ML exhibited a peak sensitivity of $6.2 \times 10^4 \%$ /RIU in Air. Though all the MLs show an enhancement in the sensitivity when operating in MOSPR mode by factors of 3 to 4, which is due to the benefit obtained through MO enhancement to overcome the losses introduced with the Co layer, the Co(16.8)/Au(28) bilayer showed a sensitivity of $1.2 \times 10^5 \%$ /RIU. Based on this comparison, one would conclude that an MOSPR sensor is preferable but ML-based MOSPR sensors do not provide an advantage compared to basic bilayer structures. Notably, however, the MOSPR sensitivity of the $N = 10$ ML in Water improved by 50% with

Table 2. Sensitivity comparison between SPR and MOSPR configurations at $\lambda = 785$ nm. In the case of the N = 1 ML, which lacks strong SPR, we report the response near the onset of TIR.

Sensor Structure Mode Units	N = 1 ML		N = 5 ML		N = 10 ML		N = 14 ML		Thick bilayer	
	TIR	MOTIR	SPR	MOSPR	SPR	MOSPR	SPR	MOSPR	SPR	MOSPR
Air	3.8×10^4	5.5×10^4	2.1×10^4	6.2×10^4	3.6×10^4	5.9×10^4	1.1×10^4	2.4×10^4	2.9×10^4	1.2×10^5
Water	2.0×10^3	2.0×10^3	5.0×10^3	1.9×10^4	1.8×10^4	3.2×10^4	6.0×10^3	9.0×10^3	2.0×10^3	2.0×10^4

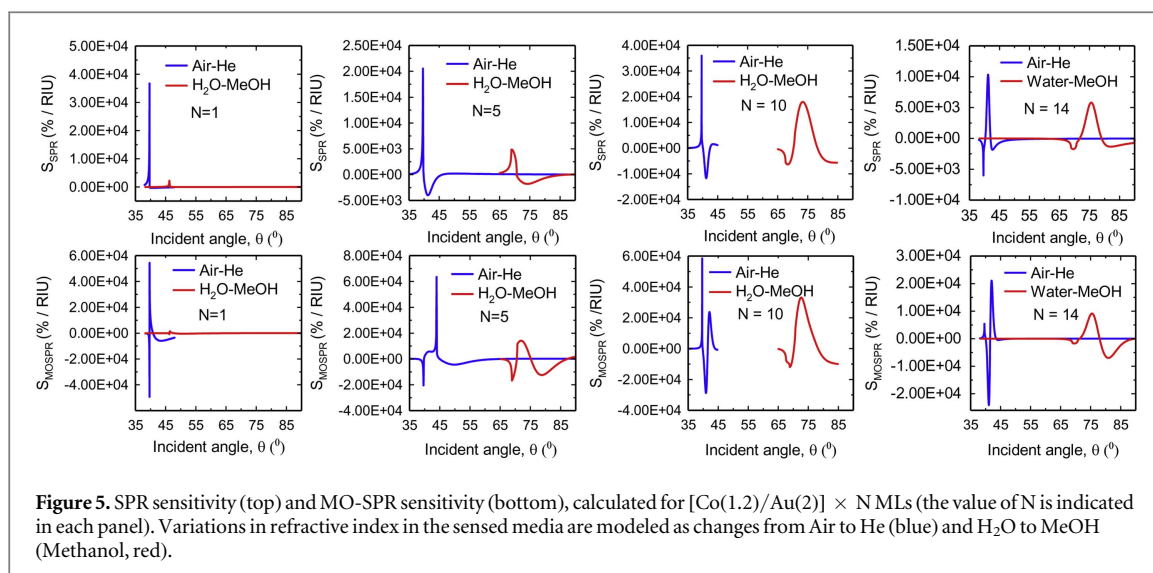


Figure 5. SPR sensitivity (top) and MO-SPR sensitivity (bottom), calculated for $[\text{Co}(1.2)/\text{Au}(2)] \times N$ MLs (the value of N is indicated in each panel). Variations in refractive index in the sensed media are modeled as changes from Air to He (blue) and H_2O to MeOH (Methanol, red).

respect to simpler bilayer structures, highlighting that the optimization based on the balance of MO enhancement and optical losses depends markedly on the dielectric medium in which the sensor is intended to operate. This is particularly important considering that the majority of biosensor applications are intended for operation in Water-based media. Further enhancements may be possible by the addition of photonic crystal structures [2].

4. Conclusions

As identified by XRD and XRR spectra, the nanoscale plasmonic Co/Au multilayers studied here showed excellent bilayer periodicity and surface roughness that improved with thermal annealing.

These structures showed excellent magneto-optic surface plasmon resonance properties. The MOSPR sensitivity is enhanced by a factor of 3 and 4 with respect to the SPR sensor in an Air-He and Water-Methanol media, respectively. Multilayer-based MOSPR sensors provide an advantage over comparable bilayer designs when operated in Water-based media, which targets common biosensing platforms.

Acknowledgments

Research at GEM Systems Inc. and York University is supported by MITACS Canada (Award: ITO 7836) and research at Center for Memory and Recording Research, UC San Diego was supported by the National Science Foundation (Award: DMR 1610538).

ORCID iDs

Conrad Rizal  <https://orcid.org/0000-0002-4599-6353>

Simone Pisana  <https://orcid.org/0000-0002-9291-6061>

References

- [1] Zvezdin A K and Kotov V A 1997 *Modern Magneto-optics and Magneto-optical Materials* (Boca Raton, FL: CRC Press)
- [2] Ignatyeva D O, Knyazev G A, Kapralov P O, Dietler G, Sekatskii S K and Belotelov V I 2016 *Sci. Rep.* **6** 28077
- [3] Kushwaha M S 2001 *J Surface Science Reports* **41** 1–416
- [4] Jain P K, Xiao Y, Walsworth R and Cohen A E 2009 *Nano Lett.* **9** 1644
- [5] Chin J Y et al 2013 *Nat. Commun.* **4** 1599
- [6] Rizal C, Niraula B and Lee H W 2016 *J Nanomed Res* **3** 00059
- [7] Rizal C and Fullerton E 2017 *J. Phys. D: Applied Physics* **50** 355002
- [8] Armelles G, Cebollada A, García-Martín A and González M U 2013 *J Advanced Optical Materials* **1** 10
- [9] Yamada A, Shirota M, Rizal C, Houga T and Ueda Y 2002 *J. of the Japan Institute of Metals* **66** 869
- [10] Ueda Y, Adachi H, Takakura W, Rizal C and Chikazawa S 2004 *Physica Status Solidi C: Conferences* **1** 1752
- [11] Rizal C, Moa B and Niraula B B 2016 *Magnetochemistry* **2** 22
- [12] Rizal C, Moa B, Wingert J and Shpyrko O G 2015 *IEEE Trans. Magn.* **51** 7
- [13] Robertson W M and Fullerton E E 1989 *J. Optical Society America B* **6** 1584
- [14] González-Díaz J B, Sepúlveda B, García-Martín A and Armelles G 2010 *Appl. Phys. Lett.* **97** 043114

- [15] Fullerton E E, Schuller I K, Vanderstraeten H and Bruynseraede Y 1992 *Phys. Rev. B* **45** 9292
- [16] Zak A K, Majid W A, Abrishami M E and Yousefi R 2011 *J Solid State Sciences* **13** 251
- [17] Cullity B D and Weymouth J W 1957 *Am. J. Phys.* **25** 394
- [18] Björck M and Andersson G 2007 *J. Appl. Crystallogr.* **40** 1174
- [19] Dekadjevi S D, Ryan P, Hickey B, Fulthorpe B and Tanner B 2001 *Phys. Rev. Lett.* **86** 5787
- [20] Springer T, Ermini M, Spackova B, Jablonku J and Homola J 2014 *Anal. Chem.* **86** 10350